*International Journal of Thermophysics, Vol. 20, No. 5, 1999*

# An Improved Guarded Parallel-Plate Method for Measuring the Thermal Conductivity of Fluids in the Critical Region

**E. P. Sakonidou,[1,2] H. R. van den Berg,[1] C. A. ten Seldam,[1] and J. V. Sengers[3,4]**

*Received November 12, 1998*

A description is presented of the construction and operating procedure of an improved guarded parallel-plate instrument for measuring the thermal conductivity of fluids in the critical region. With the improved arrangement, it has been possible to reduce the temperature differences across the fluid layer between the two horizontal plates to values as low as 0.3 mK, thus allowing the thermal conductivity of fluids to be measured at temperatures as close as 20 mK to the critical temperature. The instrument has been used to measure the thermal conductivity of methane and of a mixture of methane and ethane in the close vicinity of the critical point.

**KEY WORDS:** critical phenomena; parallel-plate method; thermal conductivity.

## 1. INTRODUCTION

There are two types of techniques for measuring the thermal conductivity of compressed fluids: dynamic methods and steady-state methods. The transient hot-wire technique [1] is the most popular dynamic method and has been developed extensively during the past two decades. This method uses a very thin wire, usually made of platinum, placed at the center of a cylindrical sample, where the wire serves both as heating element and as

[1] Van der Waals-Zeeman Instituut, Universiteit van Amsterdam, Valckenierstraat 67, 1018 XE Amsterdam, The Netherlands.

[2] Present address: Hellenic Institute of Metrology, 57022 Sindos, Thessaloniki, Greece.

[3] Department of Chemical Engineering and Institute for Physical Science and Technology, University of Maryland, College Park, Maryland 20742, U.S.A.

[4] To whom correspondence should be addressed.



0195-928X/99/0900-1339$16.00/0 

thermometer. A time-dependent perturbation in the form of a heat flux is applied to a fluid initially in equilibrium. This method is labeled transient because the power is applied abruptly and the measurement is of short duration (of the order of 1 s). The resulting temperature rise is of the order of a few kelvins, which is too large for a close approach to the critical point where convection easily develops.

In steady-state methods, a fluid layer is subjected to a stationary temperature gradient while the heat flow is measured as a function of this gradient. Two steady-state geometries have found wide acceptance: concentric cylinders and parallel plates [2]. In the first method, the fluid is enclosed between two concentric cylinders in horizontal or vertical orientation, and heat is generated in the inner cylinder. In the second method, the fluid is enclosed between two parallel plates and heat is generated in the upper plate. The possibility of convection is also present in these steady-state methods, but the parallel-plate method offers the advantage that the heat is developed from above and thus convection develops less easily. With the concentric-cylinder method the temperature difference between the inner and the outer cylinder can be reduced to about 0.3 K, which leads to reasonably accurate results for the measured thermal conductivity of the fluid at temperatures to about 3 K from the critical temperature. The parallel-plate method offers the possibility of a much closer approach ($<0.1$ K) to the critical temperature, without convective heat transfer by the use of very small temperature differences ($<1$ mK) between the upper and the lower plates, measured with thermometers of a high sensitivity. With an earlier version of our guarded parallel-plate apparatus [3], the thermal conductivity of several fluids has been measured [4–6].

In the present paper, we describe some subsequent improvements of the measuring procedure, with the purpose of increasing the ability to obtain more accurate thermal-conductivity data in the close vicinity of the critical point. Specifically, with the improved arrangements we have been able to reduce the temperature difference between the upper and the lower plates to values as small as 0.3 mK, thus enabling us to measure the thermal conductivity of fluids and fluid mixtures at temperatures as close as 20 mK to the critical temperature. The measuring arrangement described in this paper has been used to measure the thermal conductivity of pure methane and of an equimolar mixture of methane and ethane in the close vicinity of the critical point [7–9].

## 2. PRINCIPLE OF THE EXPERIMENTAL METHOD

The principle of the guarded parallel-plate cell is straightforward [2]. The sample fluid is located in a narrow gap between two horizontal plates:

an upper plate and a lower plate. The upper plate is surrounded by a guard ring and guard plate. A temperature difference across the fluid layer is established by generating heat in the upper plate. To minimize parasitic heat flows as much as possible, the guard ring and guard plate are kept at the same temperature as the upper plate by application of an appropriate amount of heat.

The thermal conductivity, $\lambda$, of the fluid between the plates is deduced from the working equation, which in its simplest form is the linearized version of the Fourier law of heat conduction:

$$\lambda = \frac{d}{A}\frac{Q}{\Delta T} \tag{1}$$

where $Q$ is the power generated in the upper plate to maintain a stationary temperature difference $\Delta T$ across the fluid layer, with thickness $d$ between the upper and the lower plates, while $A$ is the effective area of the upper plate. The ratio $d/A$ in Eq. (1) is called the cell constant. The quantities that are measured during the experiment, the dissipated power $Q_{\text{exp}}$ in the upper plate and the temperature difference $\Delta T_{\text{exp}}$ between the upper and the lower plates, are slightly different from $Q$ and $\Delta T$ in Eq. (1) as discussed in Section 6.

The guarded parallel-plate cell is enclosed in a pressure vessel, which in turn is located inside a cryostat. This design makes it possible to measure the thermal conductivity at temperatures from 77 to 335 K with pressures up to 150 MPa.

## 3. APPARATUS

### 3.1. The Thermal-Conductivity Cell

The thermal-conductivity cell, shown in Fig. 1, was designed to satisfy, as close as possible, the ideal mathematical model of pure conduction between two infinite parallel plates. The upper plate (1) consists of three parts with good mutual thermal contact, while similarly the lower plate (2), guard ring (3), and guard plate (4) each consist of two parts. These parts are made of electrolytic copper, with the guard ring and guard plate in good thermal contact. The upper plate is a cylinder 16 mm high and 38.006 mm in diameter, which contains a resistance thermometer $R_{\text{u}}$ in the lower part and a heater $S_{\text{u}}$ in the middle part. The lower plate has a height of 15 mm and a diameter of 65 mm and contains only the resistance thermometer $R_{\text{o}}$, which is located in the lower part of this plate. The guard

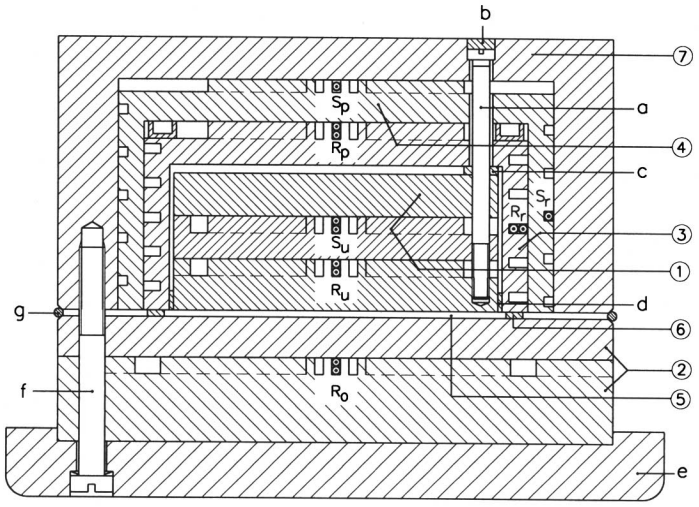


**Fig. 1.** The thermal-conductivity cell: $R_u$, $R_r$, $R_p$, and $R_o$, thermometers; $S_u$, $S_r$, and $S_p$, heaters; (1) upper plate; (2) lower plate; (3) guard ring; (4) guard plate; (5) gap; (6) glass spacers; (7) insulation cap; a and f, screws; b, insulating material; c and d, separating rings; e, mounting table; g, silk wire.

ring and guard plate are provided with resistance thermometers $R_r$ and $R_p$ in the inner parts and heaters $S_r$ and $S_p$ in the outer parts. The width of the gap (5) between the upper and the lower plates is fixed by three glass spacers (6) between the lower plate (2) and the guard ring (3). The spacers were carefully selected for equal thickness in order to reduce the risk of convection in the thermal-conductivity measurements close to the critical point. The gap width is $d = 138\ \mu$m in the present apparatus. The surfaces of the upper and lower plate that face the gap are polished flat and they are covered with a thin gold layer, which has a low thermal-emissivity coefficient so that the radiation correction on the measured thermal conductivity remains as low as possible. The guard plate and the guard ring in turn are surrounded by an insulation cap (7), made of kufalit BZH, which is a composite material consisting of araldite and powdered magnesium silicate. This material, which is a good electrical (specific resistance, $10^{12}\ \Omega \cdot$m) as well as thermal (thermal conductivity, $0.3\ \mathrm{W \cdot m^{-1} \cdot K^{-1}}$) insulator, can withstand low temperatures and high pressures, and has a thermal-expansion coefficient comparable to that of copper. This property is very important to ensure that no deformation of the cell and, hence, no change of the gap width will occur upon lowering the temperature. The upper plate (1), guard ring and guard plate (3, 4), and insulation cap (7) are screwed together with three screws (a), which are inserted in kufalit

tubes and also covered by this material (b) so that there is no direct thermal contact between the upper plate and the guard plate. The kufalit separating rings (c) around these screws and the kufalit ring (d) around the upper plate define the width of the gaps between the upper plate and the guard plate and between the upper plate and the guard ring, respectively. The total height of the guarded parallel-plate cell is 47 mm, and its diameter is 65 mm. The lower plate (2) is firmly connected to the insulation cap (7) and a small mounting table (e) with three screws (f). These screws are provided with bronze springs so that no deformation of the cell will occur under exerted tension. The mounting table is used to establish good thermal contact between the thermal-conductivity cell and the pressure vessel. A silk wire (g) around the measuring gap prevents large-scale fluid flow from the outside, and the same purpose is also served by the ring (d).

All thermometers and heaters are platinum wires with a length of about 1 m except for the thermometer in the lower plate, which has a length of 2 m. The thermometers and the heater in the upper plate have a diameter of 30 $\mu$m, while the other heaters have a diameter of 50 $\mu$m. They are located in rectangular grooves inside the plates and are electrically insulated from the copper sections by more than 1300 beads of beryllium oxide (specific resistance, $10^{14}\,\Omega \cdot \mathrm{m}$); this material is a very good thermal conductor, with a thermal conductivity at low temperatures that is higher than $500\,\mathrm{W} \cdot \mathrm{m}^{-1} \cdot \mathrm{K}^{-1}$, so that the thermal resistance between the wires and the cell is negligible. Moreover, the linear thermal-expansion coefficient of this material ($0.58 \times 10^{-5}\,\mathrm{K}^{-1}$) is lower than that of copper, which means that, upon lowering the temperature, the thermal contact between the beryllium oxide beads and the copper cell even improves. A photograph of the grooves in the lower plate of the cell together with the platinum thermometer wire $R_0$ and the beryllium oxide beads is shown in Fig. 2. All connections of the wiring from the cell to the surroundings were welded to minimize thermoelectric voltages. All wires are led through holes in the different parts of the cell, and they are insulated with Teflon tubes. These holes are closed with cone-shaped Teflon pieces in order to impede fluid flow through them.

### 3.2. Pressure Vessel and Cryostat

The thermal-conductivity cell is located inside the pressure vessel, which in turn is located inside a newly built cryostat. Since a detailed description of this equipment is given elsewhere [7], we give only a short summary here.

A platinum resistor located in the bottom of the pressure vessel serves as a temperature sensor, and it is incorporated in a Thomson bridge circuit.

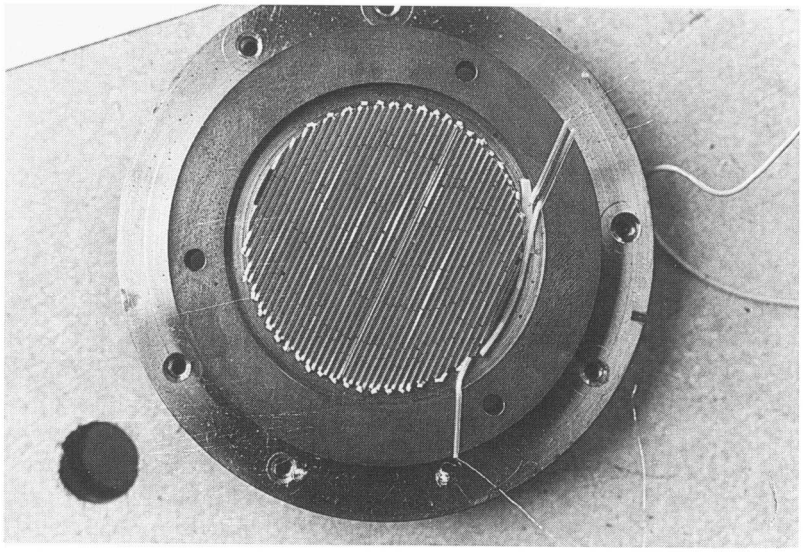

**Fig. 2.** Top view of the bottom part of the lower plate of the thermal-conductivity cell (indicated by 2 in Fig. 1) showing the grooves with the platinum thermometer wire $R_0$.

This bridge feeds a control system for the current through the main heater consisting of manganin wires at the outside wall of the cylindrical pressure vessel. A platinum thermometer also located in the bottom of the pressure vessel is used for measuring the temperature, while a second platinum thermometer mounted at the top of the pressure vessel provides information about the temperature distribution along the pressure vessel. Both thermometers have been calibrated, in the temperature range from $-100$ to $+60$°C, by the Dutch calibration organization NMI (Nederlands Meetinstituut, Delft).

A new cryostat was built for the special purpose of reducing temperature gradients in the pressure vessel under moderate cryogenic conditions. This cryostat consists of a copper cylinder with a diameter of 203 mm, which, in contrast with the original cryostat [5, 6], is shielded with an additional second copper cylinder. The space between these two cylinders is filled with Armaflex, which is a good insulating material at cryogenic temperatures. Furthermore, the extended cryostat is again directly immersed in a large Dewar vessel that contains liquid nitrogen. The inner cylinder of the new cryostat is provided with a heater, which is a thermocoax cable located in grooves machined in the cylindrical wall, and with separate resistor heaters at the top and bottom. This cylinder acts like a shield that, with the use of copper–constantan thermocouples, is maintained at a constant temperature slightly lower (0.3°C) than the

control temperature of the pressure vessel. The position of the platinum resistance thermometer in the bottom of the pressure vessel serves as a reference point in the hierarchy of the temperature control system (TCS) for the combination of the pressure vessel and cryostat.

## 4. ELECTRICAL CIRCUITS

The electrical schematic shown in Fig. 3 consists of two completely separate circuits, namely, the heater circuit and the thermometer circuit, and two smaller auxiliary circuits, the reference circuit and the Thomson bridge circuit. The parts within the gray area bounded by the broken lines in Fig. 3 are located inside the thermal-conductivity cell.

The heater circuit, shown in the lower part of Fig. 3, is designed to heat the upper plate with respect to the lower plate and also to maintain the guard ring and guard plate at the same average temperature as the upper plate. The stability of the heater power supply is better than 200 ppm at a supply voltage of 5.0 V. The heaters $S_p$ and $S_r$ are wired in parallel with the upper-plate heater $S_u$; at 295 K $S_u$, $S_r$, and $S_p$ have resistances of 38, 40, and 209 $\Omega$, respectively. The powers developed in these heaters are controlled with a personal computer (PC), interfaced with 13-bit digital–analog converter (DAC) voltage outputs, to equalize the temperatures of the upper plate and guard ring and plate within an adjustable limit as discussed in Section 5. The power $Q_{exp}$ developed in the upper plate is determined accurately and continuously by automatic measurements of the voltage drops across the calibrated Daven resistor $RN$ in Fig. 3 of 99.95 $\Omega$ at 295 K with a very small temperature coefficient ($1 \times 10^{-5}$ K$^{-1}$). For this purpose, an analog-to-digital converter (ADC) is used, which consists of a voltage-controlled oscillator (VCO) and a 16-bit counter.

The thermometer circuit indicated just above the heater circuit in Fig. 3 is an inverted Thomson bridge circuit. Its purpose is to determine accurately the temperature difference between the upper plate and the lower plate and to monitor the temperatures of the guard ring and guard plate. The upper branch of the Thomson bridge consists of the resistance thermometers $R_u$, $R_r$, and $R_p$ in series, which are balanced by the resistor $R_3$ (16,874 $\Omega$ at 295 K). The lower branch of the bridge consists of the resistance thermometer $R_o$, which is balanced by the resistor $R_4$ (10,005 $\Omega$ at 295 K) in series with the variable digital controlled resistor (DCR) $R_{sb}$ (67 $\Omega$ at 295 K). This resistor is composed of a standard Daven resistor of 50.002 $\Omega$ and 11 resistances of about $260{,}725/2^i$ $\Omega$ ($i = 0, 1, \ldots, 10$) that can be individually switched parallel to the basis resistor in every combination.

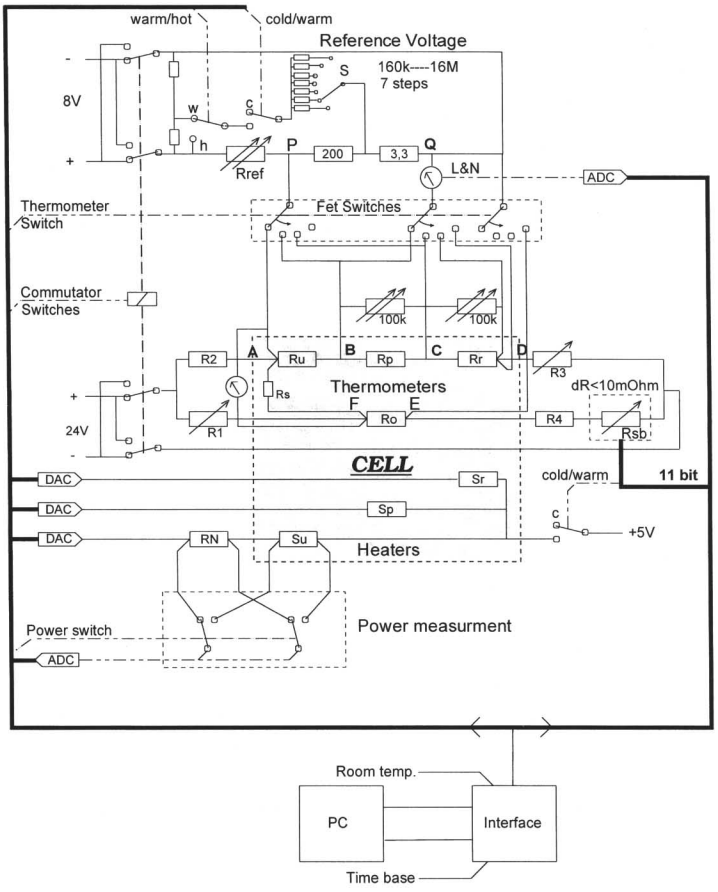


**Fig. 3.** Internal and external electrical circuits for the thermal-conductivity cell. $R_u$, $R_r$, $R_p$, and $R_o$ are platinum thermometers and $S_u$, $S_r$, and $S_p$ are heaters located in the thermal-conductivity cell as indicated in Fig. 1. $R_1$, $R_2$, $R_3$, $R_4$, $R_s$, $R_{sb}$, and $RN$ are resistors; $R_{ref}$ is a potentiometer.

This gives a total of 2047 steps that vary between 4.9 and 9.6 m$\Omega$, in which the resistance of $R_{sb}$ is reduced in total by 14.1 $\Omega$.

Very important for the thermal-conductivity measurements are the temperature coefficients of the resistance thermometers. For this reason, all thermometers were calibrated *in situ*, over the temperature range of $-82$ to $+51$°C, against the platinum resistance thermometer inserted in the bottom of the pressure vessel. The results can be represented by

$$R(t) = R(0)(1 + at + bt^2) \tag{2}$$

**Table I.** Coefficients in Eq. (2) for $R(t)$

| Thermometer | $R(0)$ ($\Omega$) | $a \times 10^6$ ($°C^{-1}$) | $b \times 10^6$ ($°C^{-2}$) |
|---|---|---|---|
| $R_u$ | 199.3366 | 3965.16 | −0.62325 |
| $R_o$ | 356.9679 | 3966.48 | −0.62449 |
| $R_r$ | 199.9086 | 3967.58 | −0.62487 |
| $R_p$ | 200.0353 | 3967.01 | −0.62563 |

where $R(t)$ is the resistance at a temperature $t$ in °C and $a$ and $b$ are coefficients. The values of these coefficients are given in Table I.

The reference circuit at the top of Fig. 3 is included to enable a comparison of the voltages $V_{AB}$, $V_{CD}$, and $V_{BC}$ across the thermometers in the upper plate and guard ring and guard plate. The reference voltage is measured across a constant resistance of 203.3 $\Omega$ to reduce the influence of the nonconstant contact resistances. This voltage $V_{PQ}$ can be changed and made equal to $V_{AB}$ by adjusting the resistance $R_{ref}$. Essential for the measuring method is that the resistances of the thermometers $R_r$ and $R_p$ initially are made equal to that of $R_u$, which is accomplished by adjusting the parallel multiturn potentiometers of 100 k$\Omega$ for $R_r$ and $R_p$. The voltage sources of 23.5 and 8.3 V for, respectively, the thermometer circuit and the reference circuit have a stability of 5 ppm. Thermoelectric voltages are eliminated by measurements with opposite current directions with the aid of four mercury wetted relays as commutators on the voltage supplies. The currents in the upper and lower branches of the Thomson bridge are about 1.29 and 2.15 mA, respectively, and nearly independent of the cell temperature.

The auxiliary bridge circuit, whose purpose is to balance the resistance of the lead wires consists of the resistor $R_2$ (755 $\Omega$ at 295 K), the variable resistor $R_1$ (451 $\Omega$ at 295 K), and the resistor $R_s$ (3 $\Omega$ at 295 K) between $R_u$ and $R_o$. The temperature difference between the upper and the lower plates is determined from the imbalance voltage $V_{DE}$ in the Thomson bridge circuit, while the comparison of the temperature in the upper plate with the temperatures of the guard ring and guard plate is accomplished by determining the differences of the voltages across $R_u$, $R_r$, and $R_p$ from the reference voltage $V_{PQ}$. The voltages over these three thermometers and the bridge voltage are selected with field effect transistor (FET) switches, measured with a Leeds and Northrup (L&N) Type 9828 Null detector, digitized with an ADC, and then processed with a PC. To reduce the effect of noise in the measurement of the different voltages, an appropriate number of determinations are averaged. This leads to a precision of 0.01 $\mu$V for the voltages over the three thermometers, which corresponds to an

uncertainty in the three relative temperatures of 10 $\mu$K, while for the bridge voltage, a precision of 0.005 $\mu$V can be reached. The sensitivity of the bridge is expressed as the change of the bridge voltage $V_{DE}$ per change of 1 m$\Omega$ of the DCR $R_{sb}$. This sensitivity drops from 0.028 $\mu$V at 308 K to 0.017 $\mu$V at 190 K, due mainly to the increase in the temperature coefficient of the thermometer in the upper plate by a factor of 1.77 in this temperature range.

When the cell is heated, the switch S in the reference circuit is closed, and consequently, the reference voltage $V_{PQ}$, which has been adjusted during the first cold stage of the measurement, is increased according to one of the seven positions of the switch. In this way, seven discrete values for the temperature difference $\Delta T$ ($\sim 1.5 \times 2^i$ mK, $i = 0, 1,...,6$) between the upper and the lower plates can be imposed. A shift between $-10$ and $+10$ mK for these values of $\Delta T$ can be applied by the introduction of an offset in the L&N measurement software of the thermometer voltages, which is necessary for imposing temperature differences smaller than 1 mK.

## 5. EXPERIMENTAL PROCEDURE

The experimental procedure for the measurements of the thermal conductivity with our guarded parallel-plate cell has now been almost completely automated and fully optimized. Before one or more measurements are initiated, the multiturn potentiometer $R_{ref}$ is adjusted so that the reference voltage $V_{PQ}$ is as close as possible equal to the voltage $V_{AB}$ across the upper-plate thermometer $R_u$ with the use of an L&N Null detector, which measures the difference between the two voltages. The voltages $V_{CD}$ and $V_{BC}$ across the guard ring $R_r$ and guard plate $R_p$ thermometers are then also made equal to $V_{PQ}$ by adjusting their respective parallel resistances. These adjustments are actually the only manual adjustments during the measurement of the thermal conductivity as the voltages across the three thermometers are subsequently measured as differences with the constant reference voltage $V_{PQ}$.

The scheme according to which the voltages across the thermometers and the bridge are measured has been optimized. Every item is measured in both current directions just one after the other before the next item is examined, and moreover, the switching goes each time via the bridge voltage. Due to this new procedure, for every amount the time interval between opposite current measurements is shortened, so that a possible drift is restricted, and since the bridge voltage is always nearly zero, the L&N amplifier recovers sooner.

A measurement of the thermal conductivity proceeds in three stages. Before the start of the first stage, values must be chosen for a set of 15 parameters in the measuring program. These parameters determining the

**Table II.** Survey of Measuring Parameters

| Parameter | Description | Symbol | Value |
|---|---|---|---|
| Integration time | Time interval during which the voltage across an item is measured | $\tau_i$ | 1 s |
| Commutation delay time | Time interval after reversing the current before voltage measurement is resumed | $\tau_d$ | 2 s |
| Number of sequences | Number of sequences for averaging measured voltages | $N_s$ | 3 |
| | Minimum number of index points | | |
| Minimum points 1 | In stage 1 | $N_{min,1}$ | 50 |
| Minimum points 2 | In stage 2 | $N_{min,2}$ | $60 \rightarrow 90$ |
| Minimum points 3 | In stage 3 | $N_{min,3}$ | $50 \rightarrow 75$ |
| | Maximum number of index points | | |
| Maximum points 1 | In stage 1 | $N_{max,1}$ | 70 |
| Maximum points 2 | In stage 2 | $N_{max,2}$ | 120 |
| Maximum points 3 | In stage 3 | $N_{max,3}$ | $70 \rightarrow 100$ |
| Bridge window | Range for bridge voltage | $\Delta V_B$ | $0.27 \rightarrow 0.18\ \mu V$ |
| Stability condition | Range for thermometer voltages | $\Delta V_{st}$ | $0.02\ \mu V$ |
| Stability points | Number of index points during which the stability condition must be fulfilled | $N_{st}$ | 60 |
| Preparation time | Time in "preparation" heating mode | $\tau_{pm}$ | $30 \rightarrow 45$ min |
| Switch position | Position of switch S for choosing the temperature difference | $P_s$ | $1 \rightarrow 7$ |
| LN offset | Offset voltage for thermometers | $\Delta V_0$ | $-1.2 \rightarrow 0.5\ \mu V$ |

duration and stability of each of the three stages are listed in Table II. The times that govern all the three stages are the integration time $\tau_i$ and the commutation delay time $\tau_d$. Since the measuring time for one voltage is 0.1 s, 10 measurements of that voltage can be made during an integration time of 1 s, which are averaged. Thus, a complete measuring sequence through the different items with $\tau_d = 2$ s will last $8 \cdot 1 + 8 \cdot 2 = 24$ s. These results are recorded in the computer, averaged over $N_s$ sequences, and stored. It means that every index point, i.e., the "time unit" of the measurement, corresponds for the case $N_s = 3$ with 72 s and contains the average voltages over the three thermometers and the bridge as well as the ambient temperature.

### 5.1. First Stage

The cell is in thermal equilibrium and the Thomson bridge is automatically brought into equilibrium, which means that the bridge voltage $V_{DE}$ is brought within the "bridge window" $\Delta V_B$ by adjusting the variable DCR $R_{sb}$ in steps of nearly 10 m$\Omega$. After $N_{min,1}$ index points have

been measured, the average bridge voltages over the first and second half of the last $N_{st}$ index points are compared. If these two values agree within the "stability condition" $\Delta V_{st}$, then the first stage is terminated. If not, this stage continues until the condition for $\Delta V_{st}$ is fulfilled. After this stage is finished, the next 10 index points are used for the calibration of the sensitivity of the bridge voltage by introducing intentionally a change of the DCR $R_{sb}$ by one step ($\sim 10\ \mathrm{m}\Omega$).

### 5.2. Second Stage

A temperature difference $\Delta T$ between the upper and the lower plates is generated and kept constant by the heating in the upper plate, while the temperatures of the guard ring and guard plate are made equal to that of the upper plate. The voltage imbalance $V_{DE}$ of the Thomson bridge is brought again within the window $\Delta V_B$ by adjusting the variable DCR $R_{sb}$. The heating of the cell evolves in three modes. In the "initial mode," the heating powers are increased stepwise until the voltage across one of the thermometers $R_u$ or $R_r$ or $R_p$ comes within $5\ \mu\mathrm{V}$ of the respective value of the first stage of the measurement, shifted according to the switch position $P_s$ plus, eventually, the offset $\Delta V_0$. Then the "preparation mode" comes into operation, where preset heating powers are used at the beginning. The transition of this mode to the final "measuring mode" is made when the voltages over *all* three thermometers $R_u$, $R_r$, and $R_p$ are stable for $\tau_{pm}$ min within $0.2\ \mu\mathrm{V}$ from their respective shifted values of the first stage. In the measuring mode, the heating power in the upper plate is kept constant and the upper plate performs as a reference for the guard ring and guard plate. This means that the voltages across $R_r$ and $R_p$ are compared with that across $R_u$ and the differences are made equal (within $0.01\ \mu\mathrm{V}$) to the respective differences in the first stage of the measurement by adjusting the heating powers in $S_r$ and $S_p$. The condition to finish the "measuring mode," and thus the second stage, is the same as for the first stage. The value for the minimum number of index points may be different, but the stability numbers $N_{st}$ and $\Delta V_{st}$ are the same.

As elucidated in Section 6, the temperature difference $\Delta T$ is calculated with Eqs. (7) and (8) from the applied change $\Delta R_{sb}$ of the resistance $R_{sb}$ and the *in situ* calibrated temperature coefficient $a'$ of the upper-plate thermometer $R_u$, where $\Delta R_{sb}$ must be corrected for the residual bridge voltage $V_{DE}$ with the use of the sensitivity of the bridge. The precision of $0.005\ \mu\mathrm{V}$ in the determination of the bridge voltage corresponds, in principle, to an uncertainty of $4\ \mu\mathrm{K}$ in $\Delta T$. In practice, this uncertainty is somewhat higher, due mainly to an eventual drift in the external parts of the electrical system under the influence of ambient temperature changes. This eventual drift,

which is restricted as much as possible, is determined and (approximately) accounted for in the final calculation of $\Delta T$ by means of a comparison between the resistance values of $R_{sb}$ in the first and third stages of the measurement.

### 5.3. Third Stage

In this reproduction of the first stage the cell returns to thermal equilibrium. This stage also uses the same stability criteria as in the first stage and, in most cases, even the same value for the minimum number of index points. The measurement values are saved on the hard disk of the PC, and they can be displayed if a detailed evaluation of the thermal history of the measurement is desirable.

### 5.4. All Stages

To stress the importance of a stable bridge voltage $V_{DE}$, and thus of a constant temperature difference $\Delta T$, the counting of index points and, consequently, the check of the fulfillment of the different criteria restart in each of the three stages, every time after an adjustment of the DCR $R_{sb}$. To exclude measurements of excessively long duration, different criteria in each of the three stages are overruled by a maximum condition. That is, when a maximum number of index points have been measured, the stage is terminated with a warning message to indicate less stable values. The total duration of a measurement under the current stability criteria varied between about 5 h for an ordinary measurement to about 8 h for a measurement near the critical point.

The use of very small temperature differences, which is required to perform measurements in the critical region, could be realized only due to the increase in the stability of the electrical circuits, the automatic temperature regulation and temperature equalization of the various parts of the cell, and the new experimental procedure as discussed above. In order to minimize the uncertainty of measurements under critical conditions with small values for $\Delta T$, the duration of these measurements was prolonged mainly via the parameters $N_{\min,2}$ and $\tau_{pm}$ of the second stage and also by reducing the bridge window $\Delta V_B$, as quantified in Table II, even though under in those conditions the system appeared to reach equilibrium faster.

In Fig. 4 we show measurements of the different voltages during the three stages of a measurement on methane [7], at a temperature 98 mK above the critical temperature and at a density equal to 89% of the critical density, with $\Delta T = 0.72$ mK and $Q = 1.20$ mW. In Fig. 4, I refers to the first stage, IIa and IIb refer to the preparation mode and the measuring mode

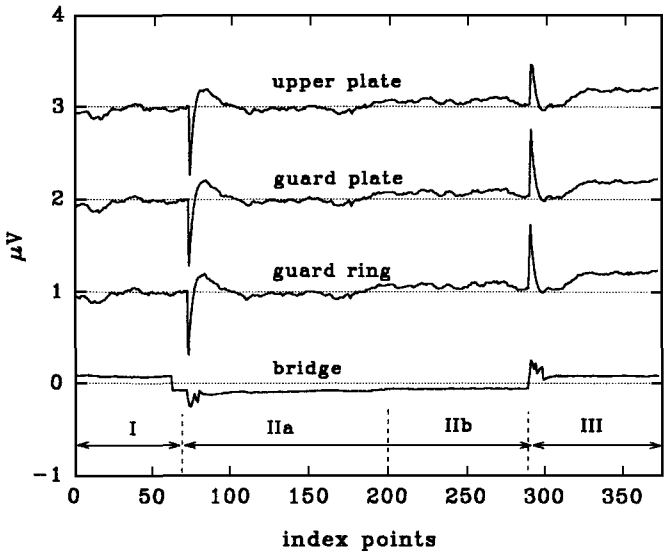


**Fig. 4.** Bridge voltage and change with respect to reference voltage across the thermometers $R_u$, $R_p$, and $R_r$ in the thermal-conductivity cell during the three stages (I, II, and III) of a measurement in the near-vicinity of the critical point of methane. The curves are separated by 1 $\mu$V ($\sim$1 mK). Measuring parameters from Table II: $N_{\min,\,1\text{-}3}$, $N_{\max,\,1\text{-}3}$, and $\tau_{pm}$, maximum values; $\Delta V_B$, minimum value.

of the second stage, respectively, and III refers to the third stage. The bridge voltage returns in the reproduction stage III to within 0.008 $\mu$V of the initial value. The small simultaneous drift in the three thermometer voltages must be ascribed to the reference voltage.

## 6. WORKING EQUATION

### 6.1. Introduction

The dimensions of the cell under the actual experimental conditions are not exactly the same as the values measured under standard conditions. Moreover, the power $Q$ in the working Eq. (1) as well as the temperature difference $\Delta T$ across the gap, differ, in general, slightly from the measured values $Q_{exp}$ and $\Delta T_{exp}$, respectively. With the various corrections the final working equation can be written

$$\lambda = \left(\frac{d}{A}\right) \frac{Q_{exp} + Q_d - Q_p - Q_r}{\Delta T_{exp} - \Delta T_l - \Delta T_r - \Delta T_a} \tag{3}$$

where $Q_d$ is a correction for additional heat dissipation in the upper plate, $Q_p$ is a correction for parasitic heat flow, $Q_r$ is a correction for radiation, $\Delta T_1$ is a correction for the location of the upper-plate thermometer, $\Delta T_r$ is a correction for residual temperature differences between the upper plate and guard ring and plate, and $\Delta T_a$ is a correction for accommodation effects. The variation of the cell constant $d/A$ with temperature has to be taken into account, but the effects of pressure are negligibly small. Corrections to the gap width and to the measured density and temperature of the fluid inside the gap, which depend on the sample fluid itself and on the experimental conditions, are discussed briefly below.

### 6.2. Corrections to the Cell Dimensions for Edge Effects, Temperature, and Absorption

The value for the plate distance $d$ is 138 $\mu$m. The area $A$ of the upper plate, with a diameter of 38.006 mm, must be corrected by 1.53% for the space between the upper plate and the guard ring in analogy with the electrical field in a Thomson capacitor [10, 11]. The corrected value for $A$ is then 1151.8 mm$^2$. The cell constant varies with temperature as

$$\frac{d}{A} = \left(\frac{d}{A}\right)_{T_{ref}} [1 + 2.72 \times 10^{-5}(T - T_{ref})] \tag{4}$$

where the value of the cell constant $(d/A)$, at a temperature $T_{ref} = 293$ K and pressure $P = 0.1$ MPa, is $(0.120 \pm 0.001)$ m$^{-1}$.

A certain amount of the sample fluid can be absorbed by the kufalit insulating material surrounding the guard ring and guard plate. By a substantial increase or decrease in the pressure in the pressure vessel, the plate distance decreases or increases slightly. This effect is temporary since the absorption or emission process in the kufalit cap gradually restores the plate distance due to swelling or shrinking of this cap. In a quantitative study, over an extended period of time on different fluids [6, 7, 9], it turned out that the observed change of the plate distance is restricted to a few percent. However, in the case of mixtures, an additional effect of this absorption process occurs, i.e., a change of the composition of the sample fluid, which may be significant [9].

### 6.3. Calculation of the Temperature Difference $\Delta T$ and Corrections

#### *6.3.1. Experimental*

Obtaining the temperature difference between the upper and the lower plates is based mainly on the application of Kirchhoff's and Ohm's laws to

the different parts of the thermometer circuit in Fig. 3. If the variable resistance $R_1$ is adjusted perfectly, so that there is no current in the wire AF that connects the upper- and lower-plate thermometers, and if, furthermore, the potential difference $V_{DE}=0$ and the thermometer resistances $R_r$ and $R_p$ are made equal to $R_u$, then one can write, respectively, for the first cold stage of the measurement and for the second stage, where the heating of the cell is activated,

$$\frac{R_5}{R_3}=\frac{R_o}{3R_u} \qquad \text{and} \qquad \frac{R_5-\Delta R_{sb}}{R_3}=\frac{R_o}{3R_u(1+a'\,\Delta T_{exp}^{(0)})} \tag{5}$$

with $R_5=R_4+R_{sb}$. Here $\Delta R_{sb}$ is the change in the resistance of $R_{sb}$ between these two stages of the measurement; $a'$ is the temperature coefficient of the upper-plate thermometer, which according to Eq. (2) is given by

$$a'=\frac{(a+2bt)}{(a+2bt+bt^2)} \tag{6}$$

with the values of the coefficients $a$ and $b$ given in Table I. From Eqs. (5) it follows that

$$\Delta T_{exp}^{(0)}=\frac{\Delta R_{sb}}{a'(R_5-\Delta R_{sb})} \tag{7}$$

which is the approximate formula for $\Delta T_{exp}$. However, one has to consider that the resistance $R_1$ cannot be adjusted perfectly and, moreover, that during heating of the upper plate the lower plate increases in temperature by an amount $\Delta T_0$. If these two corrections are taken into account, then the following expression for the temperature difference is obtained:

$$\Delta T_{exp}=\Delta T_{exp}^{(0)}(1+C_3+a'\,\Delta T_0) \tag{8}$$

where $C_3$ is an almost-constant correction

$$C_3\approx\frac{R_sR_2}{3R_u(R_1+R_2+R_s)}=0.0032 \qquad \text{(at 0°C)} \tag{9}$$

with $R_s$ the resistance of the wire AF between the upper- and the lower-plate thermometers. An estimate for the parasitic temperature rise $\Delta T_0$ will be given in Eq. (20).

*6.3.2. Corrections*

*6.3.2.1. Correction for Thermometer Location.* A small vertical temperature gradient is present in the upper plate because of the heat flow through the measuring fluid in the gap. Due to this temperature gradient, the thermometers in the upper and lower plates, which are located *inside* the plates, do not have exactly the same temperature as the surfaces facing the measuring gap. Temperature gradients also occur in the guard ring and guard plate, even when they have the same average temperature as the upper plate.

To calculate the correction $\Delta T_1$ to the experimentally measured temperature difference $\Delta T_{exp}$, an analogous electrical model has been developed for the different heat flows ($\sim$currents) and temperatures ($\sim$voltages) in the cell. This calculation, based on the real geometry of the cell and on the thermal properties of the different materials, is discussed in Appendix A. The result for the correction $\Delta T_1$, which has been computed as a function of the thermal conductivity $\lambda$ of the fluid, can be represented by

$$\Delta T_1 = F_T(\lambda)\, \Delta T_{exp} \tag{10}$$

with

$$F_T(\lambda) = \sum_{i=0}^{3} t_i \lambda^i \tag{11}$$

where the constants $t_0$ through $t_3$, with $\lambda$ expressed in $\mathrm{mW \cdot m^{-1} \cdot K^{-1}}$, are given in Table III.

The correction $F_T(\lambda)$ to the temperature difference due to the thermometer location is a monotonically rapidly increasing function of the thermal conductivity of the fluid, ranging from 1.5% for $\lambda = 50\ \mathrm{mW \cdot m^{-1} \cdot K^{-1}}$ to 12.9% for $\lambda = 500\ \mathrm{mW \cdot m^{-1} \cdot K^{-1}}$ as shown in Fig. 5.

**Table III.** Coefficients of Eqs. (11) and (17) for $F_T(\lambda)$ and $F_p(\lambda)$

| | |
|---|---|
| $t_0 = 1.51 \times 10^{-4}$ | $q_0 = 1.0945 \times 10^{-2}$ |
| $t_1 = 2.96862 \times 10^{-4}$ | $q_1 = 9.44598 \times 10^{-5}$ |
| $t_2 = -8.87435 \times 10^{-8}$ | $q_2 = -1.04515 \times 10^{-7}$ |
| $t_3 = 1.80059 \times 10^{-11}$ | $q_3 = 1.99193 \times 10^{-10}$ |
| | $q_4 = -1.88596 \times 10^{-13}$ |
| | $q_5 = 6.63124 \times 10^{-17}$ |

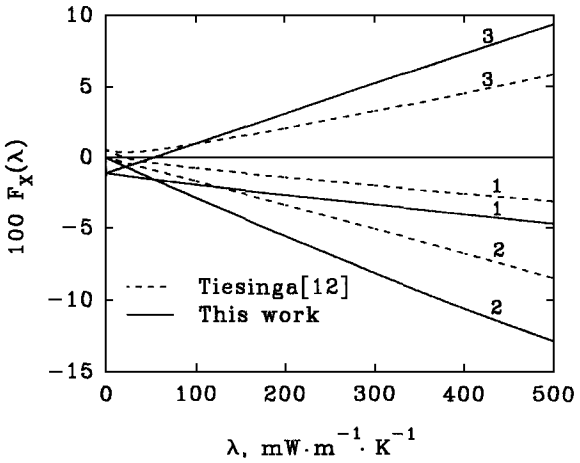


**Fig. 5.** Percentage correction $F_p(\lambda)$ for parasitic heat flow to measured power $Q$ (1), percentage correction $F_T(\lambda)$ for thermometer location (2) to measured temperature difference $\Delta T$ and percentage correction $[F_T(\lambda)-F_p(\lambda)]/[1-F_T(\lambda)]$ to the calculated thermal conductivity $\lambda$ (3). The dashed curves represent the estimates earlier calculated by Tiesinga [12], and the solid curves represent the improved results obtained in the present work.

*6.3.2.2. Correction for Parasitic Temperature Differences.* Due to the geometry of the cell, in the second stage of the measurement very small deviations remain from a complete temperature equalization between the guard ring and the upper plate. This leads to a correction $\Delta T_r$ on $\Delta T$, which is given by

$$\Delta T_r = \tfrac{1}{3}(\Delta T_{ru} + \Delta T_{pu}) \tag{12}$$

where $\Delta T_{ru}$ and $\Delta T_{pu}$ are the residual temperature differences between the guard ring and guard plate with the upper plate. The guard plate stays slightly warmer, and to compensate, the temperature of the guard ring is regulated below the temperature of the upper plate, so that the correction $\Delta T_r$ in Eq. (12) is nearly canceled. The temperature differences $\Delta T_{ru}$ and $\Delta T_{pu}$, relative to $\Delta T$, are usually less than 1% and do not exceed 2% for the recent measurements [7, 9] closest to the critical point when the threshold condition for $\Delta T$ has been satisfied.

*6.3.2.3. Correction for Accommodation.* Accommodation effects between the plates and the adjacent fluid layer become significant only

when the pressure of the fluid is very low. This effect occurs in the parallel-plate cell at both plates so that the total correction to the temperature difference according to Welander [13] can be written

$$\Delta T_a = 2\frac{2-0.83\alpha}{\alpha}\sqrt{\frac{2\pi k_B T}{m}}\frac{\lambda}{c_P + c_V}\frac{\Delta T_{exp}}{Pd} \tag{13}$$

where $\alpha$ is the accommodation coefficient, which is equal to 0.88 for a copper–fluid boundary layer [14], $P$ is the pressure of the fluid, and $c_P$ and $c_V$ are the isobaric and the isochoric specific heat capacities of the fluid, respectively. For the measurements performed with the parallel-plate cell at pressures above 1 bar, the accommodation correction never exceeds 0.5%.

## 6.4. Calculation of the Power and Corrections

### *6.4.1. Experimental*

It is easy to verify that the power dissipated in the upper plate is found from

$$Q_{exp} = V_u V_N R_N^{-1} \tag{14}$$

where $V_u$ and $V_N$ are the voltage drops across the upper-plate heater $S_u$ and the normal resistor $R_N$, respectively.

### *6.4.2. Corrections*

*6.4.2.1. Correction for Additional Heat Dissipation.* The power $Q_{exp}$ must be slightly corrected with $Q_d$ due to the additional dissipation in the leads of the heating wire $S_u$, which are located inside the upper plate but outside the joints of the potential wires. These leads have a length of about 6 mm and a diameter of 50 $\mu$m instead of, respectively, 1 m and 30 $\mu$m for $S_u$. From proportionality, it is then found that

$$Q_d = 0.0039 Q_{exp} \tag{15}$$

*6.4.2.2. Correction for Parasitic Heat Flow.* The correction to the power $Q_{exp}$ generated in the upper plate for the parasitic heat flow $Q_p$ has also been calculated from the above-mentioned analogous electrical model for the cell as discussed in Appendix A, again as a function of the thermal conductivity $\lambda$ of the sample fluid. The result of this calculation can be represented by

$$Q_p = F_p(\lambda)\, Q_{exp} \tag{16}$$

with

$$F_p = \sum_{i=0}^{5} q_i \lambda^i \tag{17}$$

where the constants $q_0$ through $q_5$, with $\lambda$ expressed in $\mathrm{mW \cdot m^{-1} \cdot K^{-1}}$, are given in Table III.

This parasitic heat-flow correction $F_p(\lambda)$ turns out to be a monotonically slowly increasing function of the thermal conductivity of the fluid, ranging from 1.6% for $\lambda = 50\ \mathrm{mW \cdot m^{-1} \cdot K^{-1}}$ to 4.7% for $\lambda = 500\ \mathrm{mW \cdot m^{-1} \cdot K^{-1}}$ as shown in Fig. 5.

*6.4.2.3. Correction for Radiation.* A small heat transport from the upper to the lower plate takes place because of radiation through the thin transparent fluid layer. The radiative power transfer is given by the Stefan–Boltzmann radiation law, which for small temperature differences reads

$$Q_r \approx 2\sigma e A T^3 \Delta T \tag{18}$$

where $\sigma$ is the Stefan–Boltzmann constant, $e$ is the emissivity of the surfaces of the upper plate and lower plates, and $T$ is the temperature of the fluid. This correction is very small for our parallel-plate cell and does not exceed 0.05%, due to the fact that the relevant surfaces inside the cell are gilded [emissivity ($=0.02$)] [15].

## 6.5. Corrections to the Density ρ and Temperature $T$

The average density of the fluid is obtained from the measured filling pressure and temperature by means of an equation of state. When the critical point is approached, the compressibility of a one-component fluid diverges and therefore a gravitationally induced density gradient develops. Because of this density gradient in the pressure vessel, and since the measuring gap in the cell is located at a position 12 mm above the bottom of the vessel, whereas the center of the volume of the vessel is 45 mm above the bottom, the density in the gap may deviate substantially from the average density, depending on the distance from the critical point [7]. In the case of fluid mixtures, gravity induces a combined density and concentration gradient near the critical point [16]. The gravitationally induced density distribution in the pressure vessel is calculated numerically from the equation of state [17].

The average temperature $T$ in the fluid layer between the upper and the lower plates differs from the temperature $T_0$ measured with the thermometer, inserted in the bottom of the pressure vessel, in the following way:

$$T = T_0 + T_s + \tfrac{1}{2}\Delta T + \Delta T_0 \tag{19}$$

where $T_s$ accounts for a temperature shift due to the nonuniformity in the heating of the pressure vessel, while the other corrections are caused by the power dissipation in the cell itself.

*6.5.1. Correction for a Temperature Shift*

It turned out that when the thermal-conductivity apparatus is operated under cryogenic conditions, a temperature shift $T_s$ must be applied to the temperature measured with the thermometer in the bottom of the pressure vessel. This temperature shift depends on the experimental conditions and partly on the nonuniform heating of the pressure vessel and, therefore, is measured separately for each fluid by an *in situ* determination of the critical temperature of the sample fluid [6, 7, 9]. An estimate of this temperature shift is presented in Appendix B.

*6.5.2. Correction for the Heating of the Upper Plate and Guard Ring and Plate*

The contributions $\frac{1}{2}\Delta T$ and $\Delta T_0$ in Eq. (19) to the average temperature $T$ account, respectively, for the temperature difference over the gap and for the temperature increase in the lower plate due to the dissipation of heat received from the upper plate and guard ring. The latter contribution was calculated with the analogous electrical model for the cell and depends on the thermal resistance between the cell and the pressure vessel and on the thermal conductivity of the sample fluid. An average is taken,

$$\Delta T_0 = \tfrac{1}{5}\Delta T \tag{20}$$

## 6.6. Final Working Equation and Experimental Uncertainty

The final working equation for the guarded parallel-plate thermal-conductivity cell can now be written

$$\lambda = \left(\frac{d}{A}\right)_{T_{\text{ref}}} [1 + 2.72 \times 10^{-5}(T - T_{\text{ref}})] \frac{Q_{\text{exp}}}{\Delta T_{\text{exp}}} \frac{1.0039 - F_{\text{p}}(\lambda) - Q_{\text{r}}/Q_{\text{exp}}}{1 - F_{\text{T}}(\lambda) - (\Delta T_{\text{r}} + \Delta T_{\text{a}})/\Delta T_{\text{exp}}} \tag{21}$$

Since the corrections depend on the thermal conductivity $\lambda$ of the measuring fluid, Eq. (21) must be solved iteratively. It should be stressed that the corrections $F_{\text{T}}(\lambda)$ and $F_{\text{p}}(\lambda)$, given by Eqs. (11) and (17), to the temperature difference $\Delta T_{\text{exp}}$ and the generated power $Q_{\text{exp}}$, respectively, have opposite effects on the calculated thermal conductivity, so that they cancel

out partially. However, at the higher thermal-conductivity values, a substantial correction ($>5\%$) remains as shown in Fig. 5. In this figure we also show the approximate corrections originally made by Tiesinga [12], as described by Mostert et al. [3], which have been applied to the thermal-conductivity measurements on argon [6]. The difference between these two net corrections increases to 5% for the higher values of $\lambda$.

The uncertainty of the measurements with our thermal-conductivity cell differs between data far away from and data close to the critical point. Outside the critical region, the uncertainty of the thermal-conductivity measurements depends primarily on the uncertainty of the plate distance $d$, which, due to the construction of the cell, could not be determined a priori on an absolute scale to better than about 5%. Therefore, this distance was derived by means of calibration measurements with respect to reference values for the thermal conductivity of argon [6]. For the cell constant $(d/A)_{293}$, the uncertainty amounts to about 1%, and for the power $Q_{\text{exp}}$ it is 0.1%, while the temperature difference $\Delta T_{\text{exp}}$ could be determined with an uncertainty of $10\,\mu$K. The uncertainty for $\Delta T_{\text{exp}}$ becomes the main source for the uncertainty of the thermal-conductivity measurements in the near-vicinity of the critical point, due to the need of using very small values for $\Delta T_{\text{exp}}$. Furthermore, the thermal conductivity becomes increasingly sensitive to errors in the local density of the fluid layer in the gap between the upper and the lower plates in the thermal-conductivity cell. It is difficult to give a precise estimate of the uncertainty of the thermal-conductivity values in the near-critical region. The thermal-conductivity data show, at a temperature within 0.14 K of the critical temperature at the critical density, a spread as large as 5% [7].

## APPENDIX A. AN ANALOGOUS ELECTRICAL MODEL FOR THE THERMAL-CONDUCTIVITY CELL

To calculate the temperatures and heat flows at different positions in the thermal-conductivity cell, we have developed an analogous electrical model for this system. In this calculation, only heat transport by conduction has been taken into account, i.e., radiation and convection have been omitted. Furthermore, we assume that this system is cylindrically symmetric, and for the calculation we partitioned the system into rings of rectangular cross section by means of cylinder surfaces and planes perpendicular to the axis. In Fig. 6, the half of a meridian cross section of the system is shown. Each of the $10 \times 7$ rectangles, with indices $(i, j)$ and bounded by dashed lines in the figure, is the cross section of a ring. Different rings can have different thermal or electrical resistances, while within a ring, the material is not necessarily homogeneous.

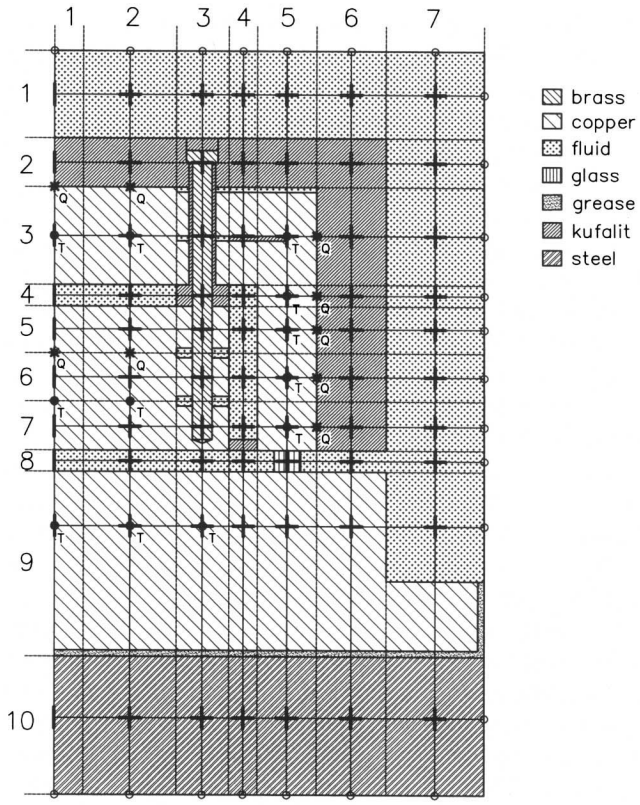


**Fig. 6.** Meridian cross section of half the thermal-conductivity cell for the calculation of the temperature distribution in the cell.

Each ring is replaced by a set of four resistors as shown in Fig. 7. $N$ and $S$ are the resistances of two rings of half the height $H$ and inner and outer radii $R_i$ and $R_u$, while $W$ and $E$ are the resistances of two cylindrical rings with height $H$ and inner and outer radii $R_i$ and $R_m$, and $R_m$ and $R_u$, respectively. In the simplest case that the rings consist of one material with thermal conductivity $\lambda$, the axial thermal resistance of $N$ or of $S$ equals

$$r_{ax} = \frac{H}{2A\lambda}, \qquad \text{with} \quad A = \pi(R_u^2 - R_i^2) \tag{A1}$$

while the radial thermal resistance of $W$ or of $E$ equals

$$r_{rad} = \int_{S_1}^{S_2} \frac{dr}{2\pi r H\lambda} = \frac{1}{2\pi H\lambda} \ln \frac{S_2}{S_1} \tag{A2}$$

with $(S_1, S_2) = (R_i, R_m)$ for $W$ and $(S_1, S_2) = (R_m, R_u)$ for $E$. The calculation of the thermal resistance of a ring is somewhat more complicated for those rings that consist of more than one material, e.g., in Fig. 6 the ring with indices (8, 5), which contains the glass spacers and the sample fluid in the measuring gap, and ring (3, 3), which contains copper, brass, kufalit, and sample fluid. If a ring consists of two layers of different thermal conductivity on top of each other, the axial thermal resistance is calculated from two resistors in series, and the radial resistance from two resistors in parallel. The opposite holds for a ring that consists of two layers parallel to the axis of the cell. A combination of these two structures also occurs for some rings. The thermal-conductivity values for the materials of the cell are $\lambda_{copper} = 388$, $\lambda_{brass} = 126$, $\lambda_{steel} = 45$, $\lambda_{glass} = 0.93$, and $\lambda_{kufalit} = 0.2\ mW \cdot m^{-1} \cdot K^{-1}$. All thermal resistances are expressed in $K \cdot W^{-1}$.

In this way, the system of the 70 cylindrical rings is replaced by a network of 260 resistors, shown by solid lines in Fig. 6. The outer ends of this network are grounded and some of the nodes are connected to current sources and other nodes to voltage meters—the electrical analogue of the heating elements and thermometers—indicated in Fig. 6 by stars and dots, respectively. The currents on the several branches of this network, as well as the potential differences, are calculated by solving the appropriate set of 156 Kirchhoff equations. The thermal conductivity of the sample fluid depends on the temperature and density; therefore, the thermal resistance

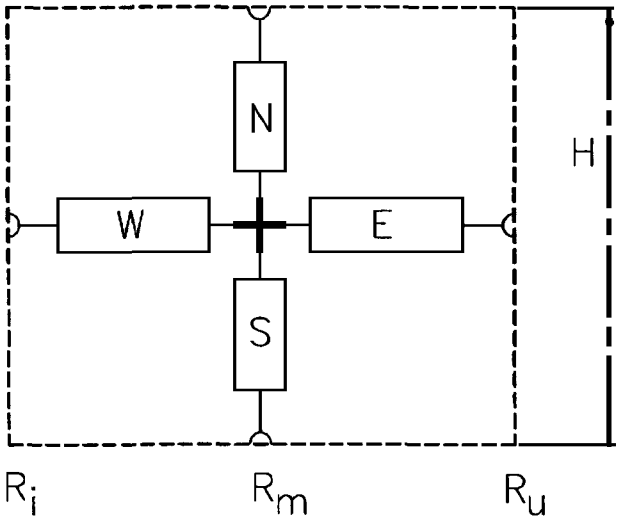


**Fig. 7.** Analogous electrical model for calculating the thermal resistance of a ring unit of the thermal-conductivity cell.

of those rings that contain the sample fluid is not a constant, which implies that the calculation for this network must be made as a function of the thermal conductivity $\lambda$ of the sample fluid. The conditions imposed on this calculation are that at the outer boundaries of the system, the voltages ($\sim$temperatures) are set to zero. Furthermore, the sources ($\sim$heaters) $Q$ in the upper plate generate a certain current. The dissipation for the current sources $Q$ in the guard ring and guard plate is then found from the minimization condition for the differences between the average values for the voltages ($\sim$temperatures) in the guard ring and guard plate on one side and the average value for the upper plate on the other side.

In Table IV, results of this calculation are given for some values of the thermal conductivity $\lambda$ of the sample fluid. The second and third columns in this table show, as a percentage of the temperature difference $\Delta T$ over the gap, the differences between the average temperatures of the guard ring and guard plate, respectively, with respect to the average temperature of the upper plate. The fourth column shows, as a percentage of the temperature difference $\Delta T$ over the gap, the temperature increase in the guard ring in the axial direction between the gap and the guard plate. The last column gives the ratio of the dissipated powers in the guard ring and upper plate. It should be mentioned that the calculated values for these ratios agree reasonably well with the measured values.

The main results of this calculation, i.e., the correction to the temperature difference $\Delta T_{\text{exp}}$, measured with the thermometers in the upper and lower plates, due to the location of these thermometers, and the correction to the dissipated power $Q_{\text{exp}}$ in the upper plate due to parasitic heat flows, are presented in Sections 6.3.2 and 6.4.2 and Fig. 5. In Fig. 8 we show some calculated temperature–contour curves for the thermal-conductivity cell for the case $\lambda = 200\ \text{mW} \cdot \text{m}^{-1} \cdot \text{K}^{-1}$, $Q_{\text{exp}} = 0.81\ \text{mW}$. The contour lines represent, on the percentage scale, $(T - T_0)/(T_{\max} - T_0)$, where $T$

**Table IV.** Calculated Values for Temperatures and Heat Flows in the Thermal-Conductivity Cell

| $\lambda$ ($\text{mW} \cdot \text{m}^{-1} \cdot \text{K}^{-1}$) | $\frac{\langle T \rangle_{\text{ring}} - \langle T \rangle_{\text{upper}}}{\Delta T}$ (%) | $\frac{\langle T \rangle_{\text{plate}} - \langle T \rangle_{\text{upper}}}{\Delta T}$ (%) | $\frac{T_{\text{ring}}(\max - \min)}{\Delta T}$ (%) | $Q_{\text{ring}}/Q_{\text{upper}}$ |
|---|---|---|---|---|
| 20 | −0.3 | +0.3 | 1.3 | 2.6 |
| 50 | −0.4 | +0.4 | 2.1 | 1.7 |
| 100 | −0.6 | +0.6 | 3.3 | 1.2 |
| 200 | −1.0 | +1.0 | 5.2 | 1.0 |
| 500 | −2.2 | +2.1 | 11.3 | 0.8 |

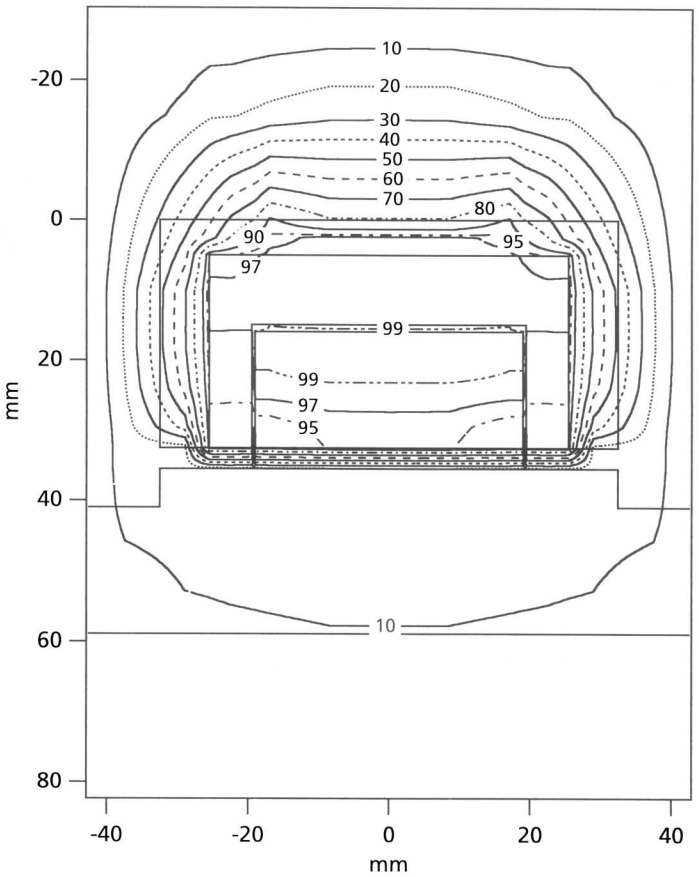


**Fig. 8.** Constant-temperature contour curves in the thermal-conductivity cell for $Q_{exp} = 0.81$ mW and a fluid thermal conductivity $\lambda = 200$ mW · $m^{-1} \cdot K^{-1}$. The numbers represent $(T - T_0)/(T_{max} - T_0)$ in percentage, where $T$ is the local temperature, $T_0$ is the measured reference temperature, and $T_{max} - T_0 = 1.00$ mK.

is the local temperature in the cell, $T_0$ is the measured reference temperature, and $T_{max} - T_0 = 1.00$ mK.

## APPENDIX B. TEMPERATURE SHIFT

The temperature $T$ of the sample fluid inside the measuring gap of the thermal-conductivity cell differs according to Eq. (19) from the temperature $T_0$ measured with the platinum resistance thermometer inserted in the

bottom of the pressure vessel. To make an estimate for the temperature shift $T_s$, the system, consisting of pressure vessel, thermal-conductivity cell, and inner cylinder of cryostat, has been simulated by a square meshed network of resistors. As with the calculation in Appendix A, it has been assumed that the system is cylindrically symmetric, where for the calculation of the thermal resistances, the thermal-conductivity values of the various materials have been taken into account. The temperature distribution over the pressure vessel was calculated by means of a two-dimensional relaxation method based on the Kirchhoff condition that the sum of the currents in each of the $23 \times 69$ nodes of the network equals zero. By means of this procedure for $T_s$, a value of about $-50$ mK has been found. Further details can be found in a Ph.D. thesis [17].

## ACKNOWLEDGMENTS

The authors acknowledge extensive support from the technical departments at the van der Waals–Zeeman Institute. Specifically, they thank J. Soede and W. Schuijlenburg for the design and assembling of the apparatus and T. Jongeneelen and P. Sannes for the development of the electronics and automation of the measuring system. H. R. van den Berg died before the manuscript was completed. P. S. van der Gulik graciously provided assistance in the final stage of the preparation of the manuscript. The research at the University of the Maryland was supported by the office of Basic Energy Sciences of the U.S. Department of Energy under Grant DE-FG02-95ER-14509.

## REFERENCES

1. M. J. Assael, C. A. Nieto de Castro, H. M. Roder, and W. A. Wakeham, in *Experimental Thermodynamics, Vol. III: Measurement of the Transport Properties of Fluids*, W. A. Wakeham, A. Nagashima, and J. V. Sengers, eds. (Blackwell Scientific, Oxford, 1991), p. 161.
2. B. Le Neindre, R. Tufeu, and A. M. Sirota, in *Experimental Thermodynamics, Vol. III: Measurement of the Transport Properties of Fluids*, W. A. Wakeham, A. Nagashima, and J. V. Sengers, eds. (Blackwell Scientific, Oxford, 1991), p. 111.
3. R. Mostert, H. R. van den Berg, and P. S. van der Gulik, *Rev. Sci. Instrum.* **60**:3466 (1989).
4. R. Mostert, Ph.D. thesis (Van der Waals Laboratory, University of Amsterdam, Amsterdam, 1991).
5. R. Mostert, H. R. van den Berg, P. S. van der Gulik, and J. V. Sengers, *J. Chem. Phys.* **92**:5464 (1990).
6. B. W. Tiesinga, E. P. Sakonidou, H. R. van den Berg, J. Luettmer-Strathmann, and J. V. Sengers, *J. Chem. Phys.* **101**:6944 (1994).
7. E. P. Sakonidou, H. R. van den Berg, C. A. ten Seldam, and J. V. Sengers, *J. Chem. Phys.* **105**:10535 (1996).

8. E. P. Sakonidou, H. R. van den Berg, C. A. ten Seldam, and J. V. Sengers, *Phys. Rev. E* **56**:R4943 (1997).
9. E. P. Sakonidou, H. R. van den Berg, C. A. ten Seldam, and J. V. Sengers, *J. Chem. Phys.* **109**:717 (1998).
10. H. S. Carslaw and J. C. Jaeger, *Conduction of Heat in Solids* (Clarendon Press, Oxford, 1947), p. 342.
11. J. C. Maxwell, *A Treatise on Electricity and Magnetism* (Dover, New York, 1954).
12. B. W. Tiesinga, Ph.D. thesis (Van der Waals Laboratory, University of Amsterdam, Amsterdam, 1980).
13. P. Welander, *Ark. Fys.* **7**:507 (1954).
14. B. G. Dickens, *Proc. Roy. Soc. A* **143**:517 (1933).
15. *Handbook of Chemistry and Physics*, 57th ed. (CRC Press, Cleveland, OH, 1977).
16. R. F. Chang, J. M. H. Levelt Sengers, T. Doiron, and J. Jones, *J. Chem. Phys.* **79**:3058 (1994).
17. E. Sakonidou, Ph.D. thesis (Van der Waals–Zeeman Institute, University of Amsterdam, Amsterdam, 1996).